

## Correlation of random wavefields: An interdisciplinary review

Eric Larose<sup>1</sup>, Ludovic Margerin<sup>1</sup>, Arnaud Derode<sup>2</sup>, Bart van Tiggelen<sup>3</sup>, Michel Campillo<sup>1</sup>, Nikolai Shapiro<sup>4</sup>, Anne Paul<sup>1</sup>, Laurent Stehly<sup>1</sup>, and Mickael Tanter<sup>2</sup>

### ABSTRACT

This paper presents an interdisciplinary review of the correlation properties of random wavefields. We expose several important theoretical results of various fields, ranging from time reversal in acoustics to transport theory in condensed matter physics. Using numerical simulations, we introduce the correlation process in an intuitive manner. We establish a fruitful mapping between time reversal and correlation, which enables us to transpose many known results from acoustics to seismology. We show that the multiple-scattering formalism developed in condensed matter physics provides a rigorous basis to analyze the field correlations in disordered media. We discuss extensively the various factors controlling and affecting the retrieval of the Green's function of a complex medium from the correlation of either noise or coda. Acoustic imaging of complex samples in the laboratory and seismic tomography of geologic structures give a glimpse of the promising wide range of applications of the correlation method.

### INTRODUCTION

Seismologists have long recognized that any seismic phase is followed or sometimes even preceded by continuous and energetic wavetrains that are difficult to interpret in terms of classical ray theory. These so-called incoherent arrivals actually represent the dominant portion of the seismic records in the short period band (frequency  $> 1$  Hz). These coda waves have been recognized as scattered waves from lateral heterogeneities in the earth. Following the work

of astrophysicists such as Milne, Schwarzschild, Chandrasekhar and van de Hulst (1980), seismologists first tried to apply radiative transfer methods to model the seismic coda waves.

In this energy transport theory, wave propagation is described simply as a random walk. The phase is assumed to be random, and wave phenomena associated with interference are assumed to be washed out. What seems left is a fully incoherent diffuse wave field, characterized by a superposition of different fields with random direction of propagation  $\mathbf{k}$ , random phase  $\phi$ , and random polarization state  $\mathbf{g}$ . Rather than the waveforms, for diffuse fields it is more convenient to consider the specific intensity of radiation, which quantifies how much energy flows on average at some time, in some direction, at some point in space. This approach successfully explained the decay rate of energy envelopes of short-period seismograms and has been applied to quantify the level of heterogeneity in different geologic settings (Sato and Fehler, 1998). Mean-free paths ranging from 200 m up to 2000 km have been reported in the same frequency bands for different regions of the earth (Margerin and Nolet, 2003; Larose et al., 2004b), which have confirmed the diffuse character of seismic coda waves.

The study of field correlation functions and intensity fluctuations was first introduced in condensed matter physics in the early 1980s. Many implicit assumptions of radiative transfer were reconsidered. The first revolution was that despite the random phase and the random wave vector, interference effects still survive in the average energy, with the observation of weak localization in electronic conduction and coherent backscattering in optics as the important paradigms. The second revolution was that fluctuations around the average (speckle) are large, sometimes even non-Gaussian, and sometimes even with infinite range. Mesoscopic studies investigated the exact spatial and temporal incoherence of the waves. On the experimental side, a clear benefit has been the many profound studies with

Manuscript received by the Editor May 25, 2005; revised manuscript received January 24, 2006; published online August 17, 2006.

<sup>1</sup>Laboratoire de Géophysique Interne et de Tectonophysique, Université Joseph Fourier and CNRS, Maison des Géosciences, BP 53, 38041 Grenoble, Cedex 9, France. E-mail: ludovic.margerin@ujf-grenoble.fr; apaul@ujf-grenoble.fr; eric.larose@obs.ujf-grenoble.fr; laurent.stehly@obs.ujf-grenoble.fr; michel.campillo@ujf-grenoble.fr.

<sup>2</sup>Laboratoire Ondes et Acoustique, Université Paris 7 and CNRS, ESPCI, 10 rue Vauquelin, 75005 Paris, France. E-mail: arnaud.derode@espci.fr; mickael.tanter@espci.fr.

<sup>3</sup>Laboratoire de Physique et Modélisation des Milieux Condensés, Université Joseph Fourier and CNRS, Maison des Magistères, BP 166, 38042, Grenoble Cedex 9, France. E-mail: bart.van-tiggelen@grenoble-cnrs.fr.

<sup>4</sup>Center for Imaging of the Earth's Interior, Department of Physics, University of Colorado at Boulder, Campus Box 390, Boulder, Colorado 80309. E-mail: nshapiro@ipgp.jussieu.fr.

© 2006 Society of Exploration Geophysicists. All rights reserved.

microwaves and ultrasound, where the phase and the field dynamics are much more accessible than for De Broglie waves or optical waves.

Today, the study of diffuse wave propagation has achieved an interdisciplinary character, and many kinds of waves are known to obey a diffusion equation (Fouque, 1999). In seismology, mesoscopic effects such as weak localization have been reported (Larose et al., 2004b), and coda wave interferometry uses the decorrelation properties of coda signal to infer temporal changes in the earth (Snieder et al., 2002). Using time reversal and multiple scattering as concepts, we investigate and analyze the correlation properties of random seismic signals. In particular, we illustrate the retrieval of the Green's function of an inhomogeneous medium with examples drawn from numerical, laboratory and field experiments.

### VISUALIZATION OF THE CORRELATION PROCESS

Here, we will illustrate some fundamental aspects of the correlation process with a numerical experiment. It will help us to visualize and interpret the emergence of the Green's function in an open medium, either homogeneous or heterogeneous. The numerical scheme is based on a 2D finite-difference simulation of the acoustic-wave equation, and absorbing boundary conditions are implemented (Joly, 1995). First let us consider two receivers,  $a$  and  $b$ , and a source  $s$ . The source emits a broadband pulse  $e(t)$  with central frequency  $f_0$  and a Gaussian envelope  $\sigma = 2/f_0$ . The numerical simulations have been performed on a spatial grid of  $\lambda_0/30$  and with a time step of  $T_0/42.5$ , where  $\lambda_0$  is the dominant wavelength and  $T_0 = 1/f_0$ . Only compressional waves are considered here, whose wave speed  $c$  equals 1500 m/s. In the following, the time-domain Green's function between  $a$  and  $b$  will be denoted  $G_{ab}(t)$ . Thus, the waveform re-

ceived by  $a$  from the source  $s$  is  $\Phi_a^{(s)}(t) = G_{sa}(t) \otimes e(t)$ , where  $\otimes$  means convolution. The correlation process consists of calculating the time integral:

$$C_{ab}^{(s)}(\tau) = \int \Phi_a^{(s)}(t) \Phi_b^{(s)}(t + \tau) dt = \Phi_a^{(s)}(-\tau) \otimes \Phi_b^{(s)}(\tau). \quad (1)$$

If a distribution of sources is used instead of a single source, the results are stacked to form:

$$C_{ab}(\tau) = \sum_s C_{ab}^{(s)}(\tau). \quad (2)$$

This operation will be referred to as *source averaging*. Visually, the correlation  $C_{ab}(\tau)$  can be displayed with snapshots of the wavefield. The receiver  $a$  and the distribution of sources  $s$  are fixed, and for a given time difference  $\tau$ , we draw a 2D map of the correlation  $C_{ab}(\tau)$  for all possible positions of point  $b$ . This is shown in Figures 1–3.

In Figure 1, a peculiar distribution of sources has been chosen: They form a closed loop around the receivers. The correlation map is represented at three different time lags:  $\tau = -3T_0$ ,  $\tau = 0$ ,  $\tau = 10T_0$ . Interestingly, these snapshots reveal something that looks like a perfect cylindrical wave converging to  $a$  for negative time lags, then diverging from  $a$  for positive time lags. If we plot the correlation  $C_{ab}(\tau)$  for a given point  $b$  as a function of the time lag  $\tau$  (Figure 1d), we see an antisymmetric waveform with two peaks that correspond exactly to  $\pm$  the arrival time  $ab/c$  of a pulse that would be traveling between  $a$  and  $b$ . This has been verified for every point  $b$  inside the loop of sources. Indeed, an instantaneous 2D map of the Green's function  $G_{ab}$  would give a cylindrical wave centered on  $a$ , exactly like what we see on the correlation snapshots at any time and for any

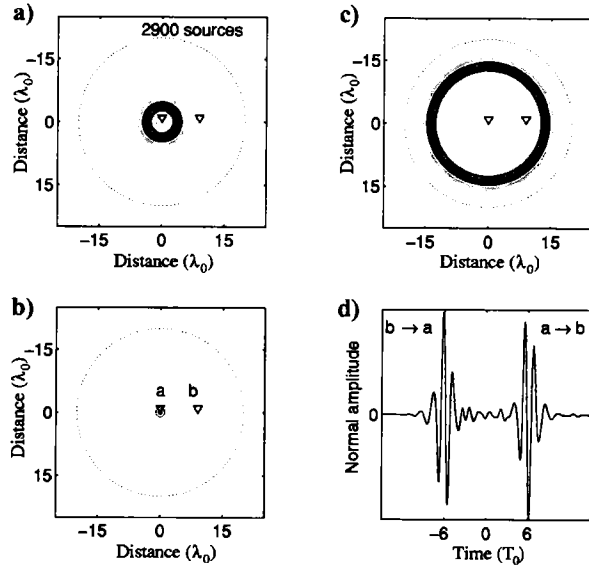


Figure 1. Map of the correlations averaged over 2900 circularly distributed sources. In (a), (b), and (c), the unit length is the wavelength  $\lambda_0$ . Maps are presented for (a) correlation times  $\tau = -3T_0$ , (b)  $\tau = 0$ , and (c)  $\tau = +10T_0$ , where  $T_0$  is the central period of oscillation. Figure 1d shows a typical correlation function for two points separated by six wavelengths. Negative (resp. positive) time corresponds to the wavefront propagating from  $b$  to  $a$  (resp. from  $a$  to  $b$ ).

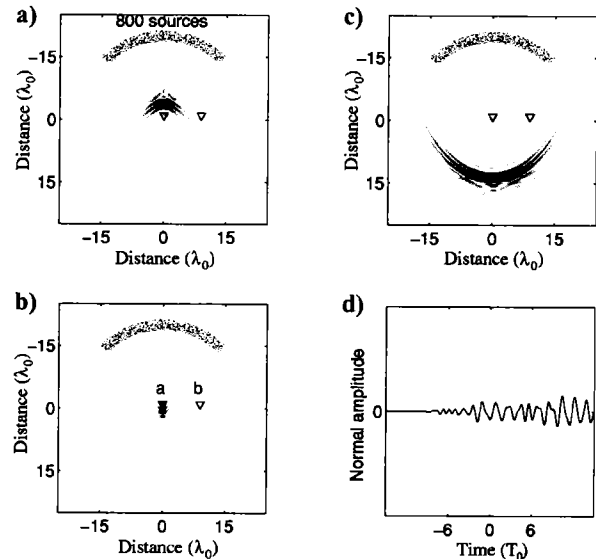


Figure 2. Map of the correlations averaged over 800 sources, randomly distributed, though asymmetrically. In (a), (b), and (c), the unit length is the wavelength  $\lambda_0$ . Maps reflect correlation times (a)  $\tau = -3T_0$ , (b)  $\tau = 0$ , and (c)  $\tau = +10T_0$ , while (d) shows a typical correlation for the same couple of points,  $a$  and  $b$ , as in Figure 1. Because of the asymmetric distribution of sources, the wavefront reconstruction is imperfect.

point  $b$ . So, for this particular distribution of sources, there is an obvious similarity between the Green's function  $G_{ab}$  and the waveform  $C_{ab}(\tau)$  obtained from passive correlation, in which the term *passive* insists on the fact that no source has been acting at either  $a$  or  $b$ .

In a second simulation, we perform a similar numerical experiment with an asymmetric distribution of sources, shown in Figure 2. The results are quite different from the first simulation. The snapshots still reveal a wave that focuses toward  $a$ , then diverges from  $a$ , but it has lost its cylindrical symmetry. As a consequence, the waveform  $C_{ab}(\tau)$  (Figure 2d) is no longer symmetrical and bears no resemblance to the Green's function  $G_{ab}$ . Actually, from the snapshots, one can guess that  $C_{ab}(\tau)$  would still show a peak at times corresponding to  $+ab/c$  or  $-ab/c$ , but only if  $b$  was lying in the region between  $a$  and the sources (for  $\tau < 0$ ) or if  $a$  were between  $b$  and the sources (for  $\tau > 0$ ). With such a distribution of sources, it is impossible to identify  $G_{ab}$  in the correlation map for an arbitrary pair  $(a, b)$  of receivers.

We now make the medium heterogeneous. We randomly add 600 scatterers (void inclusions). The signal  $\Phi_a^{(s)}(t)$  is now a complicated waveform that results from multiple scattering. As the coda of real seismograms, it lasts more than 300 periods i.e., 150 times the initial pulse duration, which is a sign of multiple scattering. If we perform the crosscorrelation using only the early arrivals of the coda (Figure 3), we see basically the same thing as in Figure 2: a portion of a cylindrical wavefront that converges to  $a$  with an angular spectrum limited by the distribution of the sources. If we perform the correlation on the late part of the coda, where multiple scattering dominates, the snapshot reveals an almost perfect cylindrical wave. Therefore, for every receiver  $b$ , the arrival time of the ballistic waves between  $a$  and  $b$  will be correctly estimated from the correlation  $C_{ab}$ . Multiple scattering can compensate for the asymmetric distribution of sources and tends to restore the cylindrical symmetry. Thus, the approximation for the Green's function from the field correlation is better when the medium contains many scatterers.

From these three examples, one can draw some preliminary conclusions. First, in the very particular case of a closed-loop distribu-

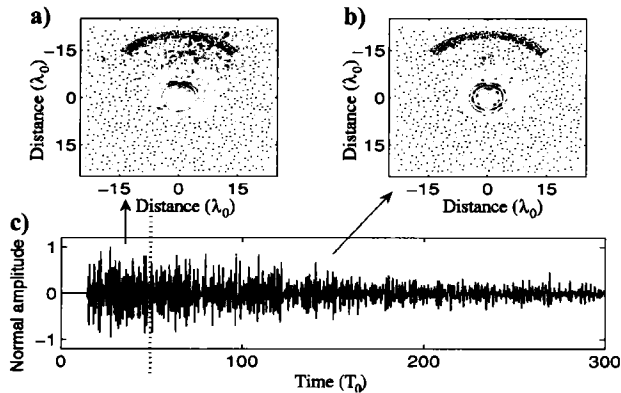


Figure 3. Map of the correlations averaged over 800 sources (same distribution as in Figure 2). Black dots are the 600 scatterers, randomly distributed in the medium (except in the central area around point  $a$ ). Maps represent correlation times  $\tau = -3T_0$ , and (c) shows a typical waveform obtained when source excitation and detection take place at  $a$ . The correlation map (a) is obtained using the first time window of (c), corresponding to waves that are not in the diffuse regime, so that all propagation directions are not equally represented. The correlation map (b) is obtained using the second time window of (c) (the late coda), corresponding to diffuse waves.

tion of sources, the Green's function  $G_{ab}$  can be retrieved either from the causal ( $\tau > 0$ ) or the anticausal ( $\tau < 0$ ) part of the correlation  $C_{ab}(\tau)$  for any pair of receivers  $a, b$  inside the loop. Secondly, if the distribution of sources differs from this ideal case, then the retrieval of the Green's function generally fails if the medium is homogeneous. Finally, in the presence of scatterers, multiple scattering seems to compensate for the lack of sources. At large lapse time in the coda, the symmetry is restored and the Green's function  $G_{ab}$  can once again be recognized in the correlation map. So it appears that disorder, randomness and scattering, which are often considered enemies, can be turned into allies. In the following sections, we develop physical arguments to interpret these results and to justify these conclusions.

### TIME REVERSAL INTERPRETATION OF THE CORRELATION PROCESS

Here we analyze the correlation experiment in terms of time-reversal (TR) arguments. Indeed, there is a strong link between the time and space correlations of a wavefield and TR (Derode et al., 2003a, b; Larose et al., 2004a). A simple physical argument based on reciprocity and TR symmetry indicates that the Green's function  $G_{ab}$  may be retrieved entirely from  $C_{ab}$ . First, as long as the medium does not move, the propagation is reciprocal, i.e.,  $G_{ab} = G_{ba}$  for any source/receiver pair  $(a, b)$ . So when  $s$  sends an ideal pulse  $e(t) = \delta(t)$  and we crosscorrelate the received responses at  $a$  and  $b$  as in equation 2, we may rewrite the result as

$$C_{ab}^{(s)}(t) = G_{sa}(-\tau) \otimes G_{sb}(\tau) = G_{as}(-\tau) \otimes G_{sb}(\tau). \quad (3)$$

Now imagine that we perform a fictitious TR experiment. Instead of being a receiver,  $a$  is now a source and sends a pulse;  $s$  records the impulse response  $G_{as}(t)$ , time-reverses it, and returns it through the unchanged medium. The resulting wavefield observed at  $b$  would then be  $G_{sa}(-t) \otimes G_{sb}(t)$  which, because of reciprocity, is exactly the crosscorrelation  $C_{ab}^{(s)}(\tau)$  of the waveforms received in  $a$  and  $b$  when  $s$  sends a pulse. So reciprocity implies that the result  $C_{ab}^{(s)}$  of the real experiment (source at  $s$ , crosscorrelate at  $a$  and  $b$ ) is the same as the result of an imaginary experiment (shoot at  $a$ , time-reverse at  $s$  and observe at  $b$ ). This is not enough, because we want to establish that the Green's function  $G_{ab}$  will appear in this crosscorrelation. Yet in the most general case,  $C_{ab}^{(s)}$  has no reason to be equal to  $G_{ab}$ .

But we can go further. Imagine now that we use several points  $s$  instead of one, and that we place them in so that they form a so-called *perfect TR mirror*: This would be the case if the sources  $s$  were continuously distributed on a surface (or a closed loop, in 2D) surrounding  $a, b$  and the heterogeneities of the medium. Then no information would be lost during the TR operation, which can be divided into two steps. During the forward step, at time  $t = 0$ ,  $a$  sends a pulse that propagates everywhere in the medium [including through  $b$  where the recorded field is  $G_{ab}(t)$ ]. It may encounter heterogeneities and is eventually recorded at every point  $s$ . The result of the TR operation is given by the backward step: If the TR device is perfect, the wave goes exactly backwards. It hits  $b$ , then refocuses at  $a$  at time  $\tau = 0$ , which implies that the field received at  $b$  (at times  $\tau < 0$ ) is exactly  $G_{ab}(-\tau)$ , the time-reversed version of the Green's function, in other words, the time-reversed version of what  $b$  has seen during the forward step. Once the pulse has refocused at  $a$ , it does not stop but diverges again from  $a$  and gives rise, at times  $\tau > 0$  to  $G_{ab}(\tau)$  at  $b$ . Thus, the exact impulse response  $G_{ab}(\tau)$  can be retrieved from either

the causal ( $\tau > 0$ ) or the anticausal part ( $\tau < 0$ ) of the averaged sum of field-field correlations.

This is exactly what we observe on the correlation maps of Figure 1, and we can reinterpret these maps as an ongoing physical process. For negative time lags (Figure 1a), what we see is a cylindrical wave converging to  $a$ : This corresponds to the first part of the backward step in the TR process. Then at  $\tau = 0$  (Figure 1b), the time-reversed wave is focused on  $a$ , and for positive time lags (Figure 1c), the cylindrical wave diverges from  $a$ . In this situation, any point  $b$  within the loop sees the pulse twice: once for positive time lags, once for negative time lags (Figure 1d).

When the distribution of sources does not form a closed loop, the symmetry between positive and negative time lags breaks. Once again, the TR analogy can be applied to interpret this result; this time the sources are not arranged as a perfect TR mirror. If the TR mirror is imperfect, it will imperfectly reconstruct the cylindrical wave as in Figure 2. Again, the correlation map may be analyzed as a snapshot of a physical process: the back propagation of a time-reversed wave. If the distribution of sources has finite extent, the corresponding TR mirror will behave as a lens with a limited aperture, which cannot recreate a perfectly cylindrical wave at its focus. In the example presented in Figure 2, it is clear that only some points  $b$  will see a sharp pulse arriving at negative times  $ab/c$ , others at a positive time  $ab/c$ , but most points will not sense anything that looks like the Green's function  $G_{ab}$ .

The most interesting situation occurs when the medium is heterogeneous. Because of the scatterers, the Green's function  $G_{ab}$  is no longer a simple pulse. It generally consists of a first arrival at time  $ab/c$  (ballistic pulse), followed by coda. The relative energy of the ballistic part and the coda depends on the distance  $ab$  and the physical properties of the scatterers, as we will recall in the next section. However, the important point is that the TR analogy is still applicable even if strong multiple scattering occurs, because its only assumption is reciprocity. Thus, even in a strongly scattering medium, the source-averaged correlation  $C_{ab}$  would reveal the exact Green's function  $G_{ab}$  (ballistic + coda) as if the sources were forming a perfect closed loop. Now, when the sources do not form a perfect TR mirror, the snapshots in Figure 3 show that the ballistic wavefront is still clearly visible and is actually better reconstructed than in a homogeneous medium, particularly when the late arrivals (the most diffracted paths) in the coda are considered. This too can be understood from what we know about TR experiments in multiple scattering media. But before we continue, we need to present some fundamentals about the physical parameters describing wave propagation in a disordered medium.

## MULTIPLE SCATTERING THEORY AND CORRELATIONS

As explained in the introduction, mesoscopic studies investigate the exact spatial and temporal coherence of the waves. An important link exists between the specific intensity in radiative transfer theory and the spatio-temporal field correlation function, which is expressed in this equation:

$$I_{\omega\mathbf{k}}(\mathbf{r}, t) = \int d\tau \exp(-i\omega\tau) \int d^3\mathbf{x} \exp(i\mathbf{k} \cdot \mathbf{x}) \\ \times \Psi\left(\mathbf{r} - \frac{1}{2}\mathbf{x}, t - \frac{1}{2}\tau\right) \Psi^*\left(\mathbf{r} + \frac{1}{2}\mathbf{x}, t + \frac{1}{2}\tau\right). \quad (4)$$

This Wigner transformation is a convenient and well-known way to track both rapid wave cycles ( $\omega$ ) and a signal envelope that evolves smoothly in space  $\mathbf{r}$  and time  $t$  (see, e.g., Ryzhik et al., 1996). In equation 4,  $\Psi$  denotes the wavefield and the specific intensity  $I$  is an explicit function of the wave-vector  $\mathbf{k}$ , which emphasizes the dependence on propagation direction. This rigorous definition in 4 avoids the phenomenological introduction of specific intensity (van de Hulst, 1980), thus facilitating a microscopic theory for  $I_{\omega\mathbf{k}}(\mathbf{r}, t)$  (Sheng, 1995; Lagendijk and van Tiggelen, 1996, and references therein; POAN Research Group, 1998; Skipetrov and van Tiggelen, 2003).

### Heuristic properties of a diffuse field

One basic characteristic property, or first principle of a diffuse wavefield is particularly important for this discussion — equipartition. Here  $\{\Psi_i\}$  is the set of normalized eigenfunctions of the (host) medium. This can always be defined in a closed linear system, but we will soon generalize to open media. The notion of a diffuse field implies the existence of some random process. For example, this process can be some random position of sources, with possible random amplitudes (noise), but it can refer also to disorder in the medium, whose nature is complex and for which we have chosen a stochastic approach, even if it is deterministic in reality. At any time, one can write the diffuse field as

$$\Psi(\mathbf{r}, t) = \sum_i a_i(t) \Psi_i(\mathbf{r}) \exp(-i\omega_i t), \quad (5)$$

where the numbers  $\{a_i(t)\}$  are complex random numbers. In the case of disorder, the numbers  $a_i$  achieve a random phase typically after a characteristic time  $\tau_i^s$ , called the *scattering mean free time of mode  $i$* , which is likely to depend on  $i$  (Trégourès and van Tiggelen, 2002). In the case of incoherent random sources, the characteristic time of the  $a_i$  is the coherence time  $\tau^c$  of the source. Dephasing can be assisted by absorption so that  $\langle a_i \rangle \rightarrow 0$  for  $t > \tau_i$  with  $1/\tau_i = 1/\tau^s + 1/\tau_i^a$ , where  $\tau_i$  and  $\tau_i^a$  stand for the extinction time and absorption time of mode  $i$ , respectively.

Let us consider a frequency bandwidth  $B$  that is much larger than the typical spacing between the eigenfrequencies. This characteristic frequency is not commonly considered in seismology because modes are not always resolved (an important exception are the low-frequency normal modes of the earth). In chaos theory, this is the inverse of the Heisenberg time  $t_H$ , which is usually the largest time in the system. The Heisenberg time equals the modal density per Hertz  $N(\omega)$  and is proportional to the volume of the medium. As a result, the bandwidth  $B$  contains many microstates, which also have achieved a finite-frequency width  $1/\tau_i$  in accordance with the uncertainty relation. Because we reasonably can assume that  $t_H \gg \tau_i$  and if we choose the bandwidth so that  $B < 1/\tau_i$ , all microstates overlap in frequency and can mode-convert by scattering from the inhomogeneities. Let  $\langle \dots \rangle$  denote ensemble average. The equipartition principle asserts that all micromodes of the random medium in  $B$  are —

on average — equally and independently populated:  $\langle a_i(t)a_j^*(t) \rangle = \sigma_B^2(t)\delta_{ij}$ , with  $\sigma_B(t)$  independent of the mode. It follows that the local average energy density is given by

$$\langle |\Psi(\mathbf{r}, t)|^2 \rangle = \sigma_B^2(t) \sum_{i \in \pm B} |\Psi_i(\mathbf{r})|^2, \quad (6)$$

where  $\sum_{i \in \pm B}$  denotes summation over both positive and negative frequencies. All modes thus contribute equally, hence, the name — equipartition. It is well known in thermodynamics, but the importance for wave scattering was only realized in the 1980s (Weaver, 1982). The equipartition regime sets in when all modes have had the time to exchange energy, which is true when the time  $t$  exceeds all mean free times  $\tau_i^f$ . The bandwidth  $B$  is a parameter that is dependent on the wave measurement and further selected by the data processing, and the present analysis applies when

$$1/t_H < B < 1/\tau_i. \quad (7)$$

The eigenmodes of a large homogeneous medium with volume  $V$  are plane waves for which  $|\Psi_i(\mathbf{r})|^2 = 1/V$  is constant in space, but clearly the equipartition argument is valid in general, particularly near boundaries where the eigenmodes are not plane waves but superpositions of different polarizations. Hennino et al. (2001) have tested the validity of equipartition of seismic waves by measuring the ratio of energies associated with different polarization. The factor  $\sigma_B^2(t)$  cancels, thus leaving a universal signature of equipartition, and thus of mode scattering.

What can we expect about the space-time correlation function of the diffuse wavefield? The earlier dephasing argument suggests that the mode numbers at different times are correlated according to  $\langle a_i(t - \frac{1}{2}\tau)a_j^*(t + \frac{1}{2}\tau) \rangle = \sigma_B^2(t)\delta_{ij} \times \exp(-|\tau|/\tau_i)$ . This generalizes equation 6 to equations 8 and 9, where a sum is performed over both negative and positive frequencies as indicated by the symbol  $\sum_{i \in \pm B}$ :

$$\begin{aligned} & \left\langle \Psi_B\left(\mathbf{r}, t - \frac{1}{2}\tau\right) \Psi_B^*\left(\mathbf{r}', t + \frac{1}{2}\tau\right) \right\rangle \\ &= \sigma_B^2(t) \sum_{j \in \pm B} \exp(-i\omega_j\tau - |\tau|/\tau_j) \Psi_j(\mathbf{r}) \Psi_j^*(\mathbf{r}'). \end{aligned} \quad (8)$$

We can compare this expression to the one for the band-limited Green's function of the wave equation applied to the host medium:

$$\begin{aligned} G_B^\pm(\mathbf{r}, \mathbf{r}', t - t') &= \int_{\pm B} \frac{d\omega}{2\pi} \exp[-i\omega(t - t')] \\ &\times \sum_j \frac{\Psi_j(\mathbf{r}) \Psi_j^*(\mathbf{r}')}{(\omega \pm i\epsilon)^2 - \omega_j^2}. \end{aligned} \quad (9)$$

Only for infinite bandwidth, the causal Green's function  $G^+$  vanishes for all  $t < t'$ , and the anticausal Green's function  $G^-$  for all  $t > t'$ . Simple algebra shows that equations 8 and 9 lead to

$$\begin{aligned} & \left\langle \Psi_B\left(\mathbf{r}, t - \frac{1}{2}\tau\right) \Psi_B^*\left(\mathbf{r}', t + \frac{1}{2}\tau\right) \right\rangle \\ &\propto \sigma_B^2(t) \times \frac{d}{d\tau} [G_B^+(\mathbf{r}, \mathbf{r}', \tau) - G_B^-(\mathbf{r}, \mathbf{r}', \tau)], \end{aligned} \quad (10)$$

at least for time differences  $\tau < \tau_i$ . Equation 10 plays a central role in this special issue. It implies that correlations reveal information of wave trajectories between the correlation points. The time derivative

guarantees that both sides of equation 10 are symmetric in time, which is true only in the equipartition regime. For thermal noise, the proportionality factor varies linearly with  $kT$ .

### Mesoscopic transport theory

As stated in the introduction, the mesoscopic approach has been very successful to model the energy decay of regional coda waves. We intend to generalize this approach to correlations of diffuse coda waves. We emphasize that in mesoscopic approaches, one tends first to consider ensemble averages and look for fluctuations later, just as in statistical physics. In seismology, the notion of ensemble average is artificial, because any disorder is quenched, and it is customary to work with the exact waveforms. In this section, we will justify the statistical approach by showing that for a typical realization, the measured correlation function has a small probability to differ from its ensemble average. As a result, the mesoscopic approach captures major features of the correlation function of a diffuse field, even if the ensemble average is not performed explicitly. Two striking examples are the time symmetry of the correlation function and the role of large bandwidth, as we discuss below.

We have discussed diffuse-mode mixing in an intuitive way. We will focus now on weak disorder that enables mode-conversion. If the random medium is much bigger than the mean free path ( $\ell_i = c_i \times \tau_i$ , where  $c_i$  is the phase velocity of mode  $i$ ), we know that average wave propagation can be described by a diffusion equation and that mesoscopic fluctuations are approximately Gaussian. For a monopole source at position  $\mathbf{r}$ , the received wave field at  $\mathbf{r}'$ , (at frequency  $\omega$ ), is described by the Green's function  $G(\mathbf{r}, \mathbf{r}', \omega)$ , which is a random function of the configuration in the ensemble of microscopic realizations of disorder. To calculate a field correlation function, one typically needs to consider  $\langle GG^* \rangle$ . Transport theory gives the following result (Legendijk and van Tiggelen, 1996),

$$\begin{aligned} & \left\langle G\left(\mathbf{r} - \frac{1}{2}\mathbf{x}, \mathbf{r}' - \frac{1}{2}\mathbf{y}, \omega - \frac{1}{2}\Omega\right) \right. \\ & \quad \times G^*\left(\mathbf{r} + \frac{1}{2}\mathbf{x}, \mathbf{r}' + \frac{1}{2}\mathbf{y}, \omega + \frac{1}{2}\Omega\right) \left. \right\rangle \\ &= \frac{\Delta G(\mathbf{x}, \omega, \Omega)}{-i\omega} \frac{\Delta G(\mathbf{y}, \omega, \Omega)}{-i\omega} \times \rho_\omega(\mathbf{r} - \mathbf{r}', \Omega), \end{aligned} \quad (11)$$

where

$$\begin{aligned} \Delta G(\mathbf{x}, \omega, \Omega) &\equiv \left\langle G\left(\mathbf{r} - \frac{1}{2}\mathbf{x}, \mathbf{r} + \frac{1}{2}\mathbf{x}, \omega - \frac{1}{2}\Omega\right) \right. \\ & \quad \left. - G^*\left(\mathbf{r} - \frac{1}{2}\mathbf{x}, \mathbf{r} + \frac{1}{2}\mathbf{x}, \omega + \frac{1}{2}\Omega\right) \right\rangle \end{aligned}$$

(we have dropped explicit reference to  $\mathbf{r}$  because we assume translational symmetry of the average medium). With the energy density  $\rho_\omega(\mathbf{r}, \mathbf{r}', \Omega)$  obeying a diffusion equation:

$$\left[ -i\Omega - D(\omega)\nabla^2 + \frac{1}{\tau^A} \right] \rho_\omega(\mathbf{r}, \mathbf{r}', \Omega) = \delta(\mathbf{r} - \mathbf{r}'), \quad (12)$$

supplemented with appropriate boundary conditions,  $1/\tau^A$  is a mode-averaged absorption rate, and  $D$  is the diffusion constant of the waves. After inverse Laplace transformation with respect to  $\Omega$ ,

one recovers the usual diffusion equation in the time domain. This equation has served already to model the seismic coda successfully (Margerin et al., 1998). The object  $\Delta G$  establishes the connection of transport theory with the result of equation 10 above, which we shall formulate in the notation introduced earlier: The average field correlation of the diffuse field between receiver  $a$  at position  $\mathbf{r} - \frac{1}{2}\mathbf{x}$  and receiver  $b$  at position  $\mathbf{r} + \frac{1}{2}\mathbf{x}$  for a source at  $s$  is proportional to the average Green's function between the two points  $a$  and  $b$ . Because we expect that  $\rho_\omega \propto N(\omega)I(s,t) \propto \omega^2$ , with  $I(s,t)$  the mean intensity of the coda in the region of correlation, equation 11 leads to

$$\left\langle \Psi_B \left( a, t - \frac{1}{2}\tau \right) \Psi_B^* \left( b, t + \frac{1}{2}\tau \right) \right\rangle \propto I(s,t) \frac{d}{d\tau} [\langle G_{ab}^+(\tau) \rangle - \langle G_{ab}^-(\tau) \rangle]. \quad (13)$$

We have assumed that within the imposed bandwidth  $B$ , the energy density  $I$  per mode varies little, which is typically true when the power spectrum of the source and the diffusion constant  $D(\omega)$  vary little over  $B$ . For monochromatic diffuse waves in random media, equation 11 between Green's function and field correlation was derived first by Shapiro (1986), and has been observed widely in experiments with microwaves (Sebbah et al., 2002) and visible light (Emiliani et al., 2003). Contrary to equation 10, equation 13 applies to open media where the diffuse energy density depends explicitly on space coordinates of source and receiver, even in the equipartition regime.

Two further observations are worthwhile. First, equation 11 shows that the crosscorrelation of two different though well-synchronized sources ( $\mathbf{y} \neq 0$ ) measured at one point ( $\mathbf{x} = 0$ ) are proportional to the mean Green's function of the waves between the sources, when averaged over the disorder. The relevance of this notion — for the seismic context where a direct ensemble average is impossible — is being studied. This provides an interesting passive way to do remote seismic sensing, already employed in near-field optics (Emiliani et al., 2003). Secondly, equation 13 can be generalized to account for a finite current from the source to the receivers, still because of an imperfectly equipartitioned wavefield. This generates a temporal asymmetry in the correlation function that appears also in seismic observations (Campillo and Paul, 2003) and in ultrasonic experiments (Malcolm et al., 2004). The diffusion equation 12 predicts an order of magnitude  $r/ct$  (with  $c$  as the wave velocity) for this asymmetry, i. e., the  $\mathbf{k}$ -vector equipartitions only algebraically in time. In contrast, different polarizations equipartition exponentially fast (Margerin et al., 2001).

### Ensemble average and mesoscopic fluctuations

The ensemble average that routinely is used in transport theory needs discussion when applied to seismic samples whose disorder clearly is frozen. Two questions arise: (1) Do we really need ensemble average and (2) how well does it describe a typical realization if no explicit average is used? As is known from statistical mechanics, the ensemble average destroys TR invariance. Yet, we have established in the previous section that a TR operation is highly efficient in a disordered medium and is also closely related to the measurement of a correlation function. The answer in statistical mechanics is that — on the one hand — TR symmetry requires infinite precision of the microscopic realization, and — on the other hand — observable quantities have only small fluctuations when the realization

changes. As in statistical mechanics, the standard method in mesoscopic physics has been always to discuss averages and average correlation functions and probability distributions over the ensemble, because the exact wave equation in a disordered sample contains too much microscopic information. The vulnerability of TR symmetry to a changing microscopic disorder has been demonstrated by Tourin et al. (2001).

The answer to the second question can be obtained from an estimate of the statistical fluctuations around the average. Let us consider one source (earthquake), band-filter the coda signal received at some distance  $r$ , and consider the correlation function,

$$C_B(\mathbf{a}, \mathbf{b}, \tau) = \int_0^\infty dt \Psi_B \left( \mathbf{a}, t - \frac{1}{2}\tau \right) \Psi_B^* \left( \mathbf{b}, t + \frac{1}{2}\tau \right). \quad (14)$$

This corresponds to the choice  $\Omega = 0$  in equation 11. It is a well known consequence of equation 12 that different frequencies dephase very rapidly in diffuse media (Shapiro, 1986). Frequencies farther apart than the Thouless frequency  $B_T \propto D/r^2$  are uncorrelated. If the applied bandwidth  $B$  largely exceeds  $B_T$  — and this is not in disagreement with the inequality 7 — we expect from Gaussian statistics (van Tiggelen, 2003) that

$$\frac{\langle \Delta C_B^2 \rangle}{\langle C_B \rangle^2} \approx \frac{B_T}{B}. \quad (15)$$

We recall that  $\langle \dots \rangle$  denotes ensemble average. Fluctuations of  $C_B$  around its average are thus suppressed by the finite bandwidth. We identify the Thouless frequency as the elementary, coherent frequency “bit,” as first done in TR (Derode et al., 2001).

The second method that tends to suppress fluctuations is an average over sources. It can be shown — and this is the answer to the first question raised above — that a homogeneous distribution of equal sources throughout the medium actually generates the genuine Green's function in equation 13, without the need to ensemble average. An omnipresent source is typically true for noise, with which passive imaging has been investigated recently in ultrasonics (Weaver and Lobkis, 2001), in helioseismology (Duvall et al., 1993), and in seismology (Shapiro et al., 2005). It is even sufficient to have a ring of delta-correlated sources surrounding the detection place to retrieve the exact Green's function (Wapenaar, 2004; Weaver and Lobkis, 2004), as illustrated in the second section, which is basically equivalent to the closed TR cavity studied by Cassereau and Fink (1992). Yet, the exact Green's function is composed of a direct coherent arrival and a traditionally called incoherent *speckle*.

Here we address the coherent arrivals and ask how much the typical speckle prevents us from seeing the direct arrivals in passive imaging. This question is much less innocent than it appears and is presently unsolved. As a source, let us adopt a random, flat, and stationary noise distribution  $s(t, \mathbf{r})$ , whose spatial correlation is smaller than the central wavelength. This is described by the correlation  $\overline{s(\omega, \mathbf{r}) s^*(\omega', \mathbf{r}')} = S(\mathbf{r}) \delta(\mathbf{r} - \mathbf{r}') \delta(\omega - \omega')$ . The bar indicates an average over the noise. The field correlation function between points  $\mathbf{a}$  and  $\mathbf{b}$  is also stationary in time and is given by

$$C_\omega(\mathbf{a}, \mathbf{b}, t) = \int d\mathbf{r}_s G(\mathbf{a}, \mathbf{r}_s, \omega) G^*(\mathbf{b}, \mathbf{r}_s, \omega) S(\mathbf{r}_s). \quad (16)$$

The fluctuations generated by the fluctuating noise have been esti-

mated recently by Weaver and Lobkis (2005). Here we consider the fluctuations in the ensemble of random configurations, whose average is proportional to  $\text{Im} G(\mathbf{a}, \mathbf{b}, \omega)$ . If we assume Gaussian statistics in this ensemble, we can estimate the mesoscopic fluctuations from

$$\frac{\langle \Delta C_\omega(\mathbf{a}, \mathbf{a})^2 \rangle}{\langle C_\omega(\mathbf{a}, \mathbf{a}) \rangle^2} = \frac{\int d\mathbf{x} \text{Im}^2 \langle G(\mathbf{x}) \rangle}{\text{Im}^2 \langle G(0) \rangle} \times \frac{\int d\mathbf{r}_s \rho^2(\mathbf{r}_s) S^2(\mathbf{r}_s)}{\left( \int d\mathbf{r}_s \rho(\mathbf{r}_s) S(\mathbf{r}_s) \right)^2} \approx \frac{2\pi\ell}{k^2} \times \frac{1}{V_s}, \quad (17)$$

where we have inserted  $\text{Im} \langle G(\mathbf{x}) \rangle = \text{sinc} kx \exp(-x/2\ell)$ , valid for three dimensions (Shapiro, 1986). The noise originating from different coherence volumes  $\ell\lambda^2/2\pi$  generates statistically independent sources. If the typical volume  $V_s$  occupied by the noise is much greater than the coherence volume, global ensemble fluctuations tend to be strongly suppressed. This means that the information retrieved from the field correlation is, with high probability, independent of the exact realization of the disorder. In the next section, we will discuss further the different factors affecting the recovery of the Green's function and the convergence of the correlation process.

### FLUCTUATIONS OF THE CORRELATION PROCESS

In this section, we discuss the correlation of random signals in a seismological context. The results, borrowed from TR and multiple scattering theory, helped us view the correlation process not only as a data-processing operation, but also as a physical process. As a result, one can understand that if the sources are distributed as a perfect TR mirror surrounding the medium, the exact Green's function  $G_{ab}$  (ballistic + coda) should emerge from the correlation  $C_{ab}$ . For acoustic waves, this was confirmed by numerical simulations where  $a$  and  $b$  were deep inside a strongly scattering medium (Derode et al., 2003b). For elastic waves, these sources must cover all possible polarizations, i.e., a combination of monopole and dipole sources, as shown by Wapenaar (2004). However, in real life, whatever type of waves, it is unrealistic to expect a perfect distribution of sources.

Usually the number of sources is limited, and distribution is asymmetric. In seismology, for instance, seismic stations ( $a, b$ ) record the displacement field at the earth's surface, but the sources ( $s$ , the earthquakes) are aligned mostly along faults. Despite the imperfections of real sources, the TR analogy still holds and helps us understand under what conditions Green's function can or cannot be retrieved from the correlations. We only have to realize that the TR device is imperfect, with a limited number of TR channels, perhaps just one. In this respect, the numerous results (Cassereau and Fink, 1992; Draeger and Fink, 1999; Fink et al., 2000; Derode et al., 2001; de Rosny and Fink, 2002; Blomgren et al., 2002) — concerning TR focusing in homogeneous or heterogeneous media with limited channels — can be applied fruitfully to the problem of retrieving  $G_{ab}$  from  $C_{ab}$ .

It is beyond our scope to reestablish these results, but we briefly review the main points in this section. As we have argued, in a TR experiment there is a forward step (propagation from  $a$  to  $b$ , record the field in  $s$ ) and a backward step (time-reverse and send back the field in  $s$ , observation of the resulting field at point  $b$ ). If the TR could be perfect, the backward step would match the forward step, which is only possible with an ideal distribution of sources. Similarly, when

the distribution of sources is not ideal, the key question to retrieval of the Green's function is: If this were a TR experiment, when (for what time lags  $\tau$ ) and where (for which receivers  $b$ ) would the backward step be almost identical to the forward step? Several aspects of the problem have been studied (Fink et al., 2000; Derode et al., 2001; de Rosny and Fink, 2002) — particularly the role of multiple scattering, the importance of the frequency bandwidth, the influence of the number of array elements (analogous to source averaging in the correlation problem), and the effect of quantization errors. The main results can be summarized as follows:

#### 1) Source averaging

In a heterogeneous medium in which different elements  $s$  of the TR mirror receive decorrelated waveforms, with an asymmetric distribution of  $N$  elements forming a limited aperture, all elements contribute coherently to the reconstruction of the waveform. As a result, the typical fluctuations of the reconstructed Green's function should decrease as  $\sqrt{N}$ .

#### 2) Multiple scattering

Time-reversal focusing is more efficient (i. e., the backward step and the forward step are more alike) in the presence of strong multiple scattering or reverberation: The focused peak is narrower in space, indicating that the angular spectrum of the recreated wavefield is wider. In other words, strong multiple scattering or reverberation virtually enhance the size of a TR device, i.e. the number of effective sources involved. This effect is noticeable when multiple scattering dominates as when the distance of propagation is large compared to the mean free path, or when the propagation time is more than the typical equipartition time. This is illustrated by Figure 3.

#### 3) Frequency averaging

Time-reversal experiments, when performed with a limited angular aperture, take advantage of a larger frequency bandwidth. For instance, in a one-channel TR experiment performed in a multiple scattering medium on a single realization of disorder, focusing cannot be achieved if the frequency band is too narrow: The remission of the phase-conjugated monochromatic wave creates a speckle pattern that is not focused back at the source. However, as the frequency bandwidth  $\Delta\omega$  is progressively enlarged, it has been shown that a TR device manages to refocus the wave through the multiple scattering slab, even with only one source (Fink, 1997). The underlying idea is that we take advantage of frequency averaging as soon as the bandwidth  $\Delta\omega$  is larger than the correlation frequency  $\delta\omega$  of the scattering medium. In a homogeneous and lossless medium,  $\Delta\omega = \delta\omega$ . But in a multiple scattering medium, the correlation frequency  $\delta\omega$  is inversely proportional to the Thouless time ( $\delta\omega$  is also often referred to as the Thouless frequency), as explained in the previous section. Because there are roughly  $\Delta\omega/\delta\omega$  decorrelated frequencies available in the spectrum, the peak-to-noise ratio can be expected to rise as  $\sqrt{\frac{\Delta\omega}{\delta\omega}}$ , if the power spectral density is flat. Hence, using a large frequency bandwidth is another way of increasing the emergence of the ballistic Green's function from the correlation of the coda. However, note that enlarging the frequency band cannot produce miracles; in particular, it cannot replace source averaging. If we want to retrieve all the details of the exact Green's function, the only solution is to have sources surrounding the medium with all possible polarizations. But if we are satisfied with a simple estimation of the first arrival of the Green's function (ballistic

- contribution), then enlarging the frequency band helps.
- 4) One-bit correlations
- Interestingly, this technique works also with one-bit correlations: Instead of recording the true waveforms, we only record and crosscorrelate their signs, i.e., a series of  $+1/-1$ . One-bit correlations produce even better results than normal correlations. Again, it has been shown previously that one-bit TR in a multiple scattering or reverberating medium gives a higher peak-to-noise ratio than a classical TR because it gives more importance to the longest scattering paths, thus artificially reinforcing multiple scattering (Derode et al., 1999). Of course, the benefit of one-bit correlation will be only effective if the recording time is significantly more than the decay time of the multiply scattered signals. For a multiple scattering slab with thickness  $L$ , the typical decay time is the Thouless time  $L^2/D$ , with  $D$  as the diffusion constant. As long as the recording time is larger than the Thouless time, the effect of one-bit digitization is to reinforce the weight of the longest and most diffracted scattering paths relatively to early arrivals. Experimental results showed that the peak-to-noise ratio is systematically higher by  $\approx 4$  dB with one-bit correlation; therefore, a smaller number of sources can be employed, which is interesting for any practical implementation of the method.

The TR analogy preliminarily indicates that to retrieve the exact Green's function from the correlations, the sources should be placed so that they completely surround the medium and the sensors, with all possible polarizations. Fortunately, multiple scattering relaxes these strong constraints at the expense of the reconstruction of direct waves in the Green's function only. In the presence of multiple scattering, only one source with only one arbitrary polarization suffices. Reconstruction stability of the ballistic part of the Green's function increases by digitizing the waveforms over just one single bit, or averaging over different frequencies. In the next section, we apply these ideas to passive imaging and detection from correlations of diffuse or random wavefields.

## APPLICATIONS

### Laboratory experiments

The first step of our passive-imaging technique is to record the field produced by distant and/or unknown sources at two different

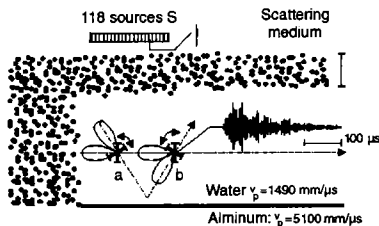


Figure 4. Experimental setup and typical waveforms. The sources  $s$  repeatedly shoot  $1 \mu\text{s}$  long pulses. Ultrasonic waves propagate through the scattering medium before reaching the sensors at  $a$  and  $b$ . An example of the raw signal obtained before the correlation process is shown. The strong attenuation of the direct wave and the long-lasting coda proves the diffuse nature of the waves, which propagate in all possible directions. The directivity pattern of the receivers is represented in thin lines. To compensate for the directivity, the receivers were rotated twice at each position to reconstruct either the direct or the reflected wavefront.

locations,  $a$  and  $b$ . It has been intensively reported that the averaged correlation of these fields yields the Green's function between  $a$  and  $b$ . In other words, this processing simulates the occurrence of a source in either  $b$  or  $a$ . In seismological applications, where sources are uncontrolled, this method provides a way of simulating sources everywhere in the medium, especially where they would not occur naturally. Additionally, the method can mimic energetic seismic sources and only requires the deployment of synchronized sensors.

In the following example, we show that it is possible to image a plane interface using the correlation technique. We develop a laboratory experiment designed to mimic seismic waves. The full size of our experimental setup is, at most, 20 cm, small enough to be improved or modified easily and rapidly. The frequency is 1 MHz, corresponding to millimeter wavelengths in water, a frequency at which ultrasound does not suffer too much from absorption. We use a collection of randomly distributed scatterers as a prototype of a multiple-scattering medium. The waves recorded in transmission through this medium are analogous to the seismic coda.

The setup of our first experiment, depicted in Figure 4, is similar to that used by Larose et al. (2004a). These authors imaged a four-layer medium using passive reconstruction of the direct acoustic wavefront from which they could infer the propagation velocities. Here, we try to reconstruct a slightly more complex Green's function: the direct wavefront and the field reflected from an interface. To this end, we use 118 aligned sources  $s$  to illuminate a scattering medium made of randomly distributed vertical steel rods. The target — a water/aluminum interface — is located behind this complex structure. The whole setup is almost 2D. The source  $s$  shoots a  $1 \mu\text{s}$  broadband pulse (3 MHz central frequency), and the recorded fields at sensors  $a$  and  $b$  are denoted by  $h_{sa}(t)$  and  $h_{sb}(t)$ , respectively. The complexity of the field, transmitted through the scattering device, is clearly visible on Figure 4, where no isolated wavefront is visible. The diffuse waves are analogous to the seismic coda.

Contrary to seismology, where sensors are pointlike and omnidirectional, the pressure measurements are achieved by means of piezoelectric transducers, whose size is not small compared to the wavelength. To compensate for the sensors' strong directivity, we need to rotate them at least twice at each acquisition. The emission/reception sequence is repeated for 12 different distances between the receivers. This provides a set of  $118 \times 12$  pairs of records for each sensor rotation angle. For any position and angle, we compute the time and source averaged two-points correlation:

$$C_{ab} = \sum_s h_{sa}(t) \times h_{sb}(t). \quad (18)$$

The results are displayed in Figure 5 where both the direct and the reflected hyperbolic-shaped wavefronts are visible. Note that without source averaging, the various arrivals are not visible. The processing of arrival times provides a precise measurement of the interface position: It lies parallel to the array, 33.2 mm from its axis. As in our previous studies, the estimated error on reconstructed travel times is of the order of one sample:  $0.05 \mu\text{s}$ , which is highly satisfactory.

### Seismic tomography from seismic noise

In the example above, we discuss the correlation fields that are produced by deterministic sources. We see that reconstruction of the Green's function relies either on a source average over a large number of sources with ad-hoc distribution, or on the equipartition resulting from multiple scattering. When equipartition is reached, all

information about the location of the source is lost. It is therefore appealing to use ambient noise, even if its actual origin is not known fully. It is noteworthy to observe that relating the correlation of noise field records to the Green's function is directly reminiscent of the fluctuation-dissipation theorem (Kubo, 1996). This relation between random fluctuations of a linear system and the system response to an external solicitation was originally formulated for thermal noise, with the equipartition principle as main argument. Indeed, there is no guarantee that the ambient seismic noise behaves as thermal noise, but we do expect that distribution of the sources of seismic noise randomizes when averaged over sufficiently long times. Furthermore, the waves that compose the noise are additionally randomized by scattering from heterogeneities, and a form of equipartition is therefore expected. The same principles must apply for diffuse coda waves from transient sources or for noise.

Using noise for exploration is not new. Aki (1957) and Toksöz (1964) proposed using noise records on an array to evaluate the phase velocity of the predominant surface waves. Using noise records to extract local propagation properties below the array has been applied successfully to investigate shallow layers that could be responsible for seismic amplification during earthquakes. Claerbout (1968) proposed ambient noise for retrieving the reflectivity response of a 1D layered structure. Recent results in helioseismology (Duvall et al., 1993; Rickett and Claerbout, 1999); acoustics (Weaver and Lobkis, 2001; Weaver and Lobkis, 2004), and seismology (Campillo and Paul, 2003; Shapiro et al., 2005) all demonstrated the validity of the approach. In seismology, limits of the method's application are not understood fully because the origin of the noise itself is not known precisely in the different frequency bands. In the low-frequency domain ( $f < 1$  Hz), the ambient noise seems dominated widely by the interaction of the ocean with the solid earth (Friederich et al., 1998; Rhie and Romanowicz, 2004). At higher frequency, the noise is produced locally by human activity and wind cannot propagate over large distances because of attenuation. In any case, the

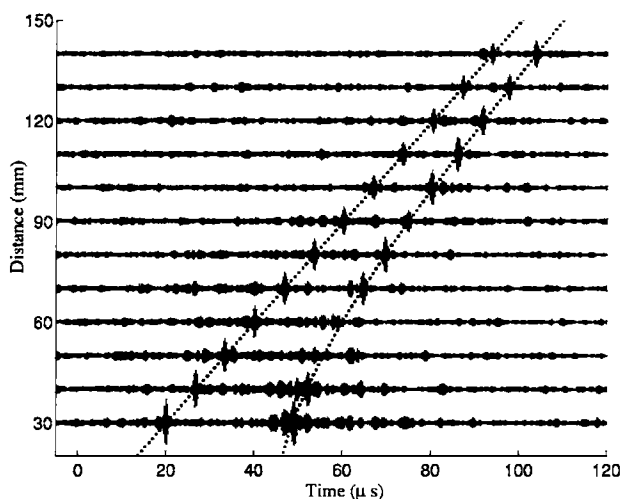


Figure 5. Example of reconstructed Green's functions obtained using 118 source-averaged correlations  $C_{ab}$ . Twelve different distances between sensors  $a$  and  $b$  are plotted, ranging from 30 mm to 140 mm. The thin dotted lines show the arrival times for the direct and reflected paths. The hyperbolic form of the reconstructed reflected wavefield matches perfectly the shape of the interface and its position, a plane interface 33.2 mm away from the sensor array.

noise is produced by surface sources, which generate predominantly surface waves. Therefore, it is expected that the signals extracted from noise records are predominantly made of surface waves. While the capability of reconstructing the body waves cannot be ruled out, it has not been convincingly demonstrated yet. Although the sources of noise are located only at the free surface, the scattering associated with topography and the strong heterogeneity of the surface layers results in a coupling between surface waves and body waves. The efficiency of this process in the earth is illustrated by the observation of the equipartition between the different modes of body and surface waves (Hennino et al., 2001).

In the seismological context, dispersive Rayleigh waves are used widely to image crustal or lithospheric shear velocity structures. We present an example using the ocean-generated noise to map Rayleigh wave group velocity following Shapiro et al. (2005). We select 30 relatively quiescent days (during which no  $M > 5.8$  earthquakes occurred) of continuous one sample per second data from 62 stations within California, from August to September 2004. We compute crosscorrelations after bandpassing the seismograms between 10 and 20 s periods. Surface-wave group speeds are estimated from the emerging Green's functions using frequency-time analysis (Levshin et al., 1989; Ritzwoller and Levshin, 1998; Shapiro and Singh, 1999) from the 1891 paths connecting these stations. We reject waveforms with signal-to-noise ratios smaller than four, and with paths shorter than two wavelengths, resulting in 785 group speed measurements at 18 s (Figure 6). We then apply a tomographic inversion (Barmin et al., 2001) to these two data sets to obtain a group speed map on a 28-km  $\times$  28-km grid across California (Figure 7). The inversion results in a variance reduction of 65% relative to the regional average speed. A resolution map is shown in Figure 8.

A variety of geologic features (Jennings, 1977) are recognizable

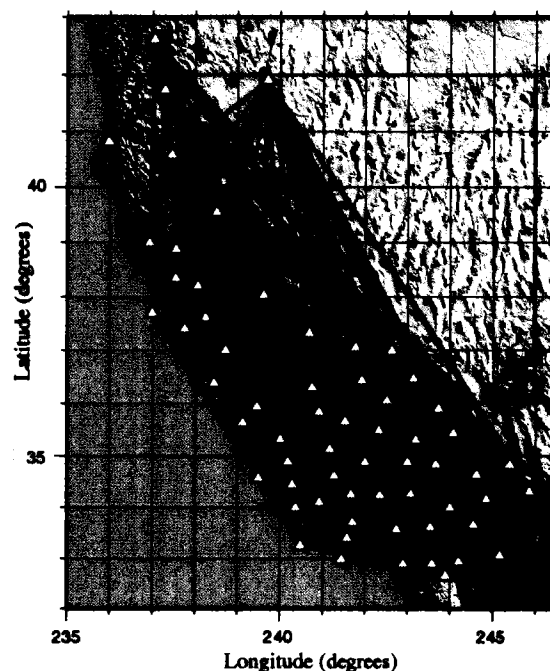


Figure 6. Paths where 18-s Rayleigh wave group speed measurements were obtained from crosscorrelations of ambient seismic noise. White triangles show locations of Usarray stations for this study.

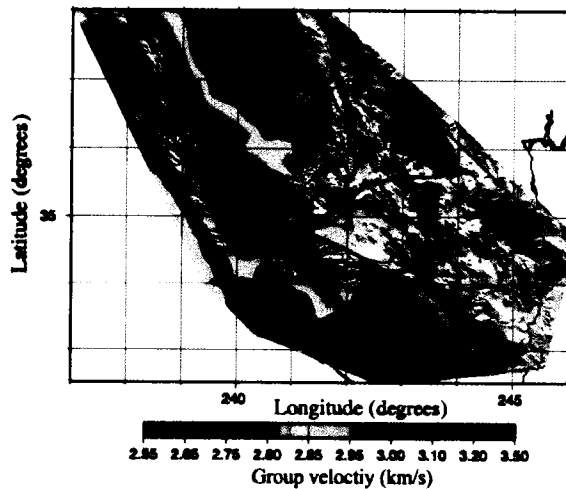


Figure 7. Rayleigh wave group speed map at 18-s period constructed by cross-correlating 30 days of ambient noise between Usarray stations. Black solid lines show known active faults. White triangles show locations of Usarray stations used in this study.

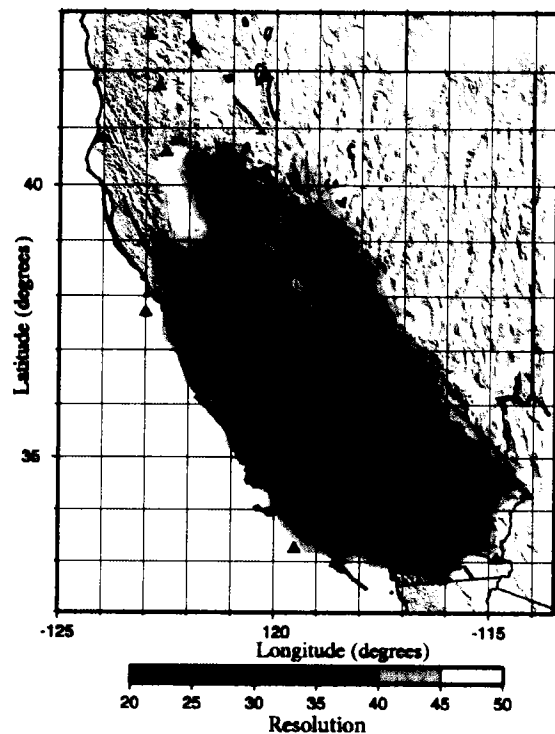


Figure 8. Resolution of the group speed map in Figure 7. Resolution worse than 50 km is denoted with the white coloration. Black solid lines are known active faults. Blue triangles are locations of the Usarray stations used in this study. The resolution was estimated with the method of Barmin et al. (2001). This method does not account for finite-frequency diffraction effects nor for off-great circle propagation and, therefore, provides rather optimistic resolution estimates. To obtain more realistic and conservative estimates, the values shown here should be multiplied by about a factor of 2.

in the estimated group speed dispersion map (Fig. 7). Rapid group speeds correspond to the remnants of the Mesozoic volcanic arc: the Sierra Nevada and the peninsular ranges composed principally of Cretaceous granitic batholiths. The group speeds are lower in the Great Basin and in the Mojave Desert, indicating that the middle crust in these areas is probably hotter and weaker than in the Sierra Nevada. Group speeds are low in the sedimentary mountain ranges, e.g., the Transverse Ranges, the southern part of the Coast Ranges, and the Diablo Range, while fast wave speeds are observed for the Salinian block. In this area, the map shows a contrast between the high-speed western wall of the San Andreas fault, composed of plutonic rocks of the Salinian block, and its low-speed eastern wall, composed of sedimentary rocks of the Franciscan formation.

## CONCLUSION

We have reviewed the correlation properties of random wavefields based on two complementary approaches, time reversal and multiple-scattering theory. We have developed an exact mapping between crosscorrelation and time-reversal operations, which provides an adequate framework to understand the emergence of the (retarded and advanced) Green's function in the correlation of coda or seismic noise. The crucial role played by multiple scattering in the reconstruction is emphasized. In particular, we have shown that increasing the bandwidth of the signals averages out the fluctuations and facilitates the extraction of the Green's function in disordered media. We also relate the observed time asymmetry of the correlation to the existence of a net energy flux in the seismic coda. In the case of elastic waves, we also point out that averaging over sources yields the exact Green's function, provided that the sources are a combination of monopoles and dipoles. We apply the theory to the imaging of heterogeneous structures in the laboratory and in the earth without the use of active sources. In both cases, the key point of the method relies on the extraction of an approximation of the Green's function of the medium from the most random parts of the signals — noise and coda waves. We show that any seismic station located at the surface of the earth can be used as a fictitious seismic source, thus increasing the number of available paths to do tomography with seismic arrays. Because the wavepaths are totally confined within the target medium, no assumptions have to be made regarding propagation outside the array. The passive imaging technique is totally free from location or timing errors and, as shown in the Californian example, greatly enhances the resolution of tomographic images.

In spite of the already demonstrated efficiency of this approach, there are still many challenging issues to solve. For example, we still have no conclusive examples of extraction of body waves from random seismic signals. Because the correlation process mimics surface sources, it is not surprising that the correlation signal is dominated by surface waves. Yet, we expect that coda waves are composed of an equipartition mixture of body and surface waves. The absence of body waves in the correlation signal might be an indicator of insufficient averaging, or it might reflect different attenuation properties of surface and body waves in the earth. We have identified several factors improving the quality of the Green's function reconstruction: large numbers or volumes of available sources, broadband signals, and multiple scattering. This last factor is particularly worth noting because it is often considered a nuisance in classical imaging approaches. The limitations of the method still need better quantification. This is a topic of ongoing research.

## REFERENCES

- Aki, K., 1957, Space and time spectra of stationary stochastic waves, with special reference to microtremors: *Bulletin of Earthquake Research Institute*, **35**, 415–456.
- Barmin, M. P., M. H. Ritzwoller, and A. L. Levshin, 2001, A fast and reliable method for surface wave tomography: *Pure and Applied Geophysics*, **158**, 1351–1375.
- Blomgren, P., G. Papanicolaou, and H. Zhao, 2002, Super-resolution in time-reversal acoustics: *Journal of the Acoustical Society of America*, **111**, 230–248.
- Campillo, M., and A. Paul, 2003, Long-range correlation in the seismic coda: *Science*, **299**, 547–549.
- Cassereau, D., and M. Fink, 1992, Time-reversal of ultrasonic fields-Part III: Theory of the closed time-reversal cavity: *IEEE Transactions on Ultrasonics, Ferroelectrics, and Frequency Control*, **39**, 579–592.
- Claerbout, J. F., 1968, Synthesis of a layered medium from its acoustic transmission response: *Geophysics*, **33**, 264–269.
- Derode, A., A. Tourin, and M. Fink, 1999, Ultrasonic pulse compression with one-bit time reversal through multiple scattering: *Journal of Applied Physics*, **85**, 6343–6352.
- , 2001, Random multiple scattering of ultrasound, Part I and II: *Physical Review E*, **64**, 6606–6618.
- Derode, A., E. Larose, M. Campillo, and M. Fink, 2003a, How to estimate the Green's function of a heterogeneous medium between two passive sensors? Application to acoustic waves: *Applied Physics Letters*, **83**, 3054–3056.
- Derode, A., E. Larose, M. Tanter, J. de Rosny, A. Tourin, M. Campillo, and M. Fink, 2003b, Recovering the Green's function from field-field correlations in an open scattering medium: *Journal of the Acoustical Society of America*, **113**, 2973–2976.
- de Rosny, J., and M. Fink, 2002, Overcoming the diffraction limit in wave physics using a time-reversal mirror and a novel acoustic sink: *Physical Review Letters*, **89**, 4301–4304.
- Draeger, C., and M. Fink, 1999, One-channel time reversal in chaotic cavities: Theoretical limits: *Journal of the Acoustical Society of America*, **105**, 611–625.
- Duvall, T. L., S. M. Jefferies, J. W. Harvey, and M. A. Pomerantz, 1993, Time-distance helioseismology: *Nature*, **362**, 430–432.
- Emiliani, V., F. Intonti, M. Cazayous, D. S. Wiersma, M. Colocci, F. Aliev, and A. Legendijk, 2003, Near-field short range correlation in optical waves transmitted through random media: *Physical Review Letters*, **90**, 250801.
- Fink, M., 1997, Time reversal of acoustic waves: *Physics Today*, **50**, 34–40.
- Fink, M., D. Cassereau, A. Derode, C. Prada, P. Roux, M. Tanter, J. L. Thomas, and F. Wu, 2000, Time-reversed acoustics: *Reports of Progress in Physics*, **63**, 1933–1994.
- Fouque, J. P., ed., 1999, *Diffuse waves in complex media*: Kluwer Academic Publishers.
- Friederich, A., F. Kruger, and K. Klinge, 1998, Ocean-generated microseismic noise located with the GRFO array: *Journal of Seismology*, **2**, 47–64.
- Hennino, R., N. P. Tregoures, N. M. Shapiro, L. Margerin, M. Campillo, B. A. van Tiggelen, and R. L. Weaver, 2001, Observation of equipartition of seismic waves: *Physical Review Letters*, **86**, 3447–3450.
- Jennings, C. W., 1977, *Geologic map of California*: California Division of Mines and Geology, Map No. 2.
- Joly, P., 1995, Absorbing boundary conditions for the finite element solution of 3D Maxwell's Equation: *IEEE Transactions on Magnetics*, **14**, 1696–1701.
- Kubo, R., 1966, The fluctuation-dissipation theorem: *Reports of Progress in Physics*, **29**, 255–284.
- Legendijk, A., and B. A. van Tiggelen, 1996, Resonant multiple scattering of light: *Physics Reports*, **270**, 143–215.
- Larose, E., A. Derode, M. Campillo, and M. Fink, 2004a, Imaging from one-bit correlations of wideband diffuse wave fields: *Journal of Applied Physics*, **95**, 8393–8399.
- Larose, E., L. Margerin, B. A. van Tiggelen, and M. Campillo, 2004b, Weak localization of seismic waves: *Physical Review Letters*, **93**, 048501.
- Levshin, A. L., T. B. Yanovskaya, A. V. Lander, B. G. Bukchin, M. P. Barmin, L. I. Ratnikova, and E. N. Its, 1989, Recording, identification, and measurement of surface wave parameters, in V. I. Keilis-Borok, ed., *Seismic surface waves in a laterally inhomogeneous earth*: Kluwer Academic Publisher, 131–182.
- Malcolm, A. E., J. Scales, and B. A. van Tiggelen, 2004, Extracting the Green's function from diffuse, equipartitioned waves: *Physical Review E*, **70**, 015601.
- Margerin, L., M. Campillo, B. A. van Tiggelen, 1998, Radiative transfer and diffusion of waves in a layered medium: new insight into coda Q: *Geophysical Journal International*, **134**, 596–612.
- Margerin, L., and G. Nolet, 2003, Multiple scattering of high-frequency seismic waves in the deep Earth: PKP precursor analysis and inversion for mantle granularity: *Journal of Geophysical Research*, **108**, 2514.
- Margerin, L., B. A. van Tiggelen, and M. Campillo, 2001, Effect of absorption on energy partition of elastic waves in the seismic coda: *Bulletin of the Seismological Society of America*, **91**, 624–627.
- POAN Research Group, 1998, *New aspects of electromagnetic and acoustic wave diffusion*: Springer Verlag.
- Rhie, J., and B. Romanowicz, 2004, Excitation of Earth's continuous free oscillation by atmosphere-ocean-seafloor coupling: *Nature*, **431**, 552–555.
- Rickett, J., and J. F. Claerbout, 1999, Acoustic daylight imaging via spectral factorization: helioseismology and reservoir monitoring: 69th Annual International Meeting, SEG, Expanded Abstracts, 1675–1678.
- Ritzwoller, M. H., and A. L. Levshin, 1998, Eurasian surface wave tomography: Group velocities: *Journal of Geophysical Research*, **103**, 4839–4878.
- Ryzhik, L., G. Papanicolaou, and J. B. Keller, 1996, Transport equations for elastic and other waves in random media: *Wave Motion*, **24**, 327–370.
- Sato, H., and M. Fehler, 1998, *Seismic wave propagation and scattering in the heterogeneous earth*: Springer, Berlin.
- Sebbah, P., B. Hu, A. Z. Genack, R. Pnini, and B. Shapiro, 2002, Spatial-field correlation: the building block of mesoscopic fluctuations: *Physical Review Letters*, **88**, 123901.
- Shapiro, B., 1986, Large intensity fluctuations for wave propagation in random media: *Physical Review Letters*, **57**, 2168–2171.
- Shapiro, N. M., and M. Campillo, L. Stehly, and M. H. Ritzwoller, 2005, High-resolution surface-wave tomography from ambient seismic noise: *Science*, **307**, 1615–1618.
- Shapiro, N. M., and S. K. Singh, 1999, A systematic error in estimating surface-wave velocity dispersion curves and a procedure for its correction: *Bulletin of the Seismological Society of America*, **89**, 1138–1142.
- Sheng, P., 1995, *Introduction to wave scattering, localization and mesoscopic phenomena*: Academic Press.
- Skipetrov, S. E., and B. A. van Tiggelen, eds., 2003, *Wave scattering in complex media, from theory to applications*, NATO ASI Vol. 107: Kluwer Academic Publishers.
- Snieder, R., A. Grêt, H. Douma, and J. Scales, 2002, Coda wave interferometry for estimating nonlinear behavior in seismic velocity: *Science*, **295**, 2253–2255.
- Toksöz, M. N., 1964, Microseisms and an attempted application to exploration geophysics: *Geophysics*, **29**, 154–177.
- Tourin, A., A. Derode, and M. Fink, 2001, Sensitivity to perturbations of a time-reversed acoustic wave in a multiple scattering medium: *Physical Review Letters*, **87**, 274301.
- Tregoures, N. P., and B. A. van Tiggelen, 2002, Quasi 2D transport of elastic waves: *Physical Review E*, **66**, 036601.
- van de Hulst, H. C., 1980, *Multiple light scattering*, Vols. 1 and 2: Academic Press.
- van Tiggelen, B. A., 2003, Green function retrieval and time reversal in a disordered world: *Physical Review Letters*, **91**, 243904.
- Wapenaar, K., 2004, Retrieving the elastodynamic Green's function of an arbitrary inhomogeneous medium by crosscorrelation: *Physical Review Letters*, **93**, 254301.
- Weaver, R. L., 1982, On diffuse waves in solid media: *Journal of the Acoustical Society of America*, **71**, 1608–1609.
- Weaver, R. L., and O. I. Lobkis, 2001, Ultrasonics without a source: Thermal fluctuation correlations at MHz frequencies: *Physical Review Letters*, **87**, 134301.
- , 2004, Diffuse fields in open systems and the emergence of the Green's function: *Journal of the Acoustical Society of America*, **116**, 2731–2734.
- , 2005, Fluctuations in diffuse field-field correlations and the emergence of the Green's function in open systems: *Journal of the Acoustical Society of America*, **117**, 3432–3439.